



Architecture, stress state and permeability of a fault zone in Jiulishan coal mine, China: Implication for coal and gas outbursts



Wei Li^{a,b,c,e,*}, Tianwei Ren^{a,b}, Andreas Busch^c, S.A.M. den Hartog^c, Yuanping Cheng^{a,b,*}, Wei Qiao^d, Bin Li^{a,b}

^a Key Laboratory of Gas and Fire Control for Coal Mines, Ministry of Education, China University of Mining and Technology, Xuzhou 221116, China

^b National Engineering Research Center for Coal Gas Control, China University of Mining and Technology, Xuzhou 221116, China

^c Heriot-Watt University, Lyell Centre, Research Avenue S, Edinburgh EH14 4AS, UK

^d Colliery Engineering Geological Research Institute, School of Resources and Earth Science, China University of Mining and Technology, Xuzhou 221116, China

^e Postdoctoral Workstation, Wanbei Coal Electricity Group Limited Liability Company, Suzhou 234000, Anhui, China

ARTICLE INFO

Keywords:

Coal mining
Fault zone
Permeability structure
Stress rotation
Coal and gas outburst

ABSTRACT

The Mafangquan (MFQ) fault zone, transecting a coal seam in Jiulishan coal mine in Jiaozuo coalfield, Henan Province, China, was investigated in detail in view of coal mining safety, including its architecture, stress and permeability features and implication for coal and gas outburst. 10 boreholes have been drilled for formation testing as well as coal sample retrieval for laboratory analysis. Gas content, Protodyakonov strength, gas emission index and pore volume are tested and analysed at different distances from the MFQ fault. A fault structure that can be separated into three distinct zones, including the fault core, the mylonitized zone and the granulated/cataclastic zone, was identified. In-situ stress tests, numerical simulations and model predictions show a principal stress rotation and fault zone stress regime. It is found that the maximum principal stress has shifted to a lower angle pent to the fault zone extend direction gradually with a destress zone from fault core to the damage zone. The permeability of the fault zone has a correlation to fault zone architecture and stress regimes in the coal seam with a high permeability in the mylonitized coal zone. The coal weakened due to deformation, high pore pressure and stress superimposition have a negative impact on coal and gas outburst. In particular, the stress rotation limits the formation of hydrofractures in the case of high pore pressure and reduces fault zone strength, which may have an orthogonal relation to the mining galleries, favouring coal and gas outburst.

1. Introduction

Coal plays an important role in the Chinese energy mix; in 2017, China consumed 50% of the worldwide coal, and around 45% of that was mined within China. With the depths of subsurface mining continuously increasing, coal mining accidents become more precarious causing thousands of fatalities in China every year Wang et al. (2014). Internationally, coal outbursts have been recognized as one of the most catastrophic failures associated with the coal mining industry. It poses one of the highest safety and productivity risks in coal mines, since outbursts have the potential to cause injuries and fatalities for miners as well as significant production losses. A recent outburst occurred in the Jiulishan coal mine during tunnel excavation adjacent to the Mafangquan (MFQ) normal fault in Jiaozuo, on October 27, 2011. About 3246 tons of solids and 291,200 m³ of coal gas was released, and 18

miners were killed (An and Cheng, 2014).

Research indicates that > 90% of significant outbursts have been concentrated in strongly deformed zones along the axes of structures such as asymmetrical anticlines, the hinge zones of recumbent folds, and the intensely deformed zones of strike-slip, thrust, reverse, and normal faults (Cao et al., 2001; Li, 2001; Li et al., 2003; Mark, 2018; Shepherd et al., 1981). In particular, coal and gas outbursts have often been reported to be closely related with faults in coal mining areas (Karacan et al., 2008; Li et al., 2011; Zhai et al., 2016). However, little research has been published focusing specifically on the architecture, stress state and permeability of fault zones and coal seams near fault zones. Fault zones are of particular importance to estimate reservoir permeability because, depending on their architecture, they enhance or impede permeability of the rock (Faulkner et al., 2010; Wibberley et al., 2008). Caine et al. (1996) developed a conceptual fault zone model that

* Corresponding authors at: National Engineering Research Center of Coal Gas Control, China University of Mining & Technology, Xuzhou, Jiangsu 221116, China.
E-mail addresses: lweisafety@cumt.edu.cn (W. Li), ypcheng@cumt.edu.cn (Y. Cheng).

is composed of the core zone and surrounding damage zones with different properties and thicknesses. A simple conceptual model for fault zone structure involves strain that is localized in a fault core surrounded by a distributed zone of fractures and faulting in the damage zone. The fault core generally consists of gouge, cataclasite or ultra-cataclasite (or a combination thereof). The damage zone generally consists of fractures over a wide range of length scales and subsidiary faults. Although this conceptual model is widely accepted, it does not apply to all rock types, in particular not to porous sandstone (Caine and Minor, 2009; Rawling and Goodwin, 2006).

In the original fault core and damage zone model of fault architecture the fault core was visualised as providing an across-fault barrier to flow and the fractured damage zone as an along/up-fault conduit. Fault slip can lead to reduce effective mechanical rock properties, such as uniaxial compressive strength, Young's modulus or brittle strain of a fault zone. At the same time permeability of the rock mass can be increased (Evans et al., 1997), or reduced due to the formation of compaction bands whereby mechanical rock strength properties increase in the vicinity of the band (Fossen and Bale, 2007). Fault zones are important since displacements can greatly reduce the strength of the coal seam due to the creation of weaker zones and the presence of gouge materials that may be dissolved and become permeable to gas and water (Karacan et al., 2011; Wu et al., 2004). The stress history of fault gouge, particularly clay-rich gouge, has been shown to be an important control on the across-fault permeability (Bolton et al., 1998; Moustafa et al., 2016). The permeability of fault cores is controlled by gouges and mineral composition; a strong deformation of localized, fine-grained fault core may have a lower permeability (Crawford et al., 2008; Marone and Scholz, 1989; Zhang and Tullis, 1998). In addition, clay-rich material tends to have lower permeabilities than quartz and/or framework silicate-rich gouges (Faulkner and Rutter, 2001; van der Zee and Urai, 2005). The permeability of fault damage zones is governed by the host rock permeability and the presence and geometric composition of both macro-scale fracture networks, and of low permeability deformation and compaction bands (Balsamo et al., 2010; Lunn et al., 2008). Some studies have shown that fault zone permeability is highly heterogeneous both spatially and temporally, may have a relationship with discrete pathways for fluid flow (Fairley and Hinds, 2004), pore pressure differential along the fault zone with time (Wiprut and Zoback, 2002), and the effective principal stress change (Cuisiat et al., 2010). Furthermore, the testing conditions with the principal stress orientation can also have an impact on the fault zone permeability (Losh and Haney, 2006).

The presence of fault zones in coal has an important implication for coal and gas outburst predictions and precaution (Fisne and Esen, 2014); however, in comparison to fault zones in siliciclastic or carbonate-rich rocks, limited information is available on the fault architecture, stress state and permeability of fault zones in coal mines. Coal is mainly composed of organic material, originating from discrete organic plant constituents, hence differs in composition from the fault zones in siliciclastic or carbonate rocks discussed above. Moreover, coal seams are dual porosity reservoirs that consist of porous matrix and fracture networks that are mechanically weaker than other sedimentary rocks (An et al., 2013). In this paper, a detailed study of the MFQ coal fault zone within the Jiaozuo coal mining area is presented. The MFQ fault is exposed in a mining gallery at a depth of 200–250 m, overlain by Quaternary strata. Since it is not possible to identify fault architecture from the fault outcrop alone, Outcrop studies were combined with in-situ well tests, coal sample analysis and numerical simulation to analyse the architecture, permeability and stress regimes of the MFQ coal fault zone, and consequently the implication for coal and gas outbursts.

2. Geological setting

Geographically, the Jiaozuo coalfield is situated in the northeast of the city of Jiaozuo, Henan province, as shown in Fig. 1 and is part of the

Late Paleozoic coal basin. Structurally it is at the southern margin of the Taihang fault-uplift zone, generated in the North China plate, which turns from nearly a NNE direction to an EW direction (Ji et al., 2017; Zhang et al., 2009). Tectonic structures north of the Fenghuangling Ridge fault (Fig. 2), which is a divisional fault of the Jiaozuo mining area, show NE and NNE directional features. This is the main fault direction in the coalfield which is dominated by high angle normal faults. The Jiulishan coal mine is located in the centre of the Jiaozuo coalfield, while the specific tectonic position is in the centre of the triangular fault block, which was formed by three faults: the Jiulishan, Fenghuangling and Fangzhuang faults. The coalfield displays a stratum strike of N50°–70°E, a SE dip direction, and a dip angle of 4–14°, representing a monoclonal structure (Ji et al., 2017).

The MFQ fault zone pinches out gradually in the NW, is cut by the Beibeidian fault in the SE and extends over 17 km in length. The fault throw over this distance varies from 45 to 165 m. It is a normal fault with strike angles between 45° and 55° and dip angles of 70° to the NW. Formation beddings gently dip to the SE at angles varying from 10° to 15°.

The strata in the Jiulishan coalfield is composed of Ordovician Majiagou (O_2f) formation, the Pennsylvanian Benxi (C_2b) and Taiyuan (C_3t) formations, the Permian Shanxi (P_1S), Xiashihezi (P_1X), and Shangshihezi (P_2S) formations. Tertiary (T) and Quaternary (Q) deposits have covered the entire Jiulishan coalfield. The main coal-bearing strata are C_3t and P_1S . Furthermore, the No. 2 coal seam in the Shanxi formation is the primary coal bed mined in this area (Fig. 2). It has an average thickness of 5.3 m and an average maximum vitrinite reflectance ($R_{o,max}$) of 3.5% (Zhang et al., 2009). It was further found that the No. 2 coal seam poses an increased risk of coal and gas outbursts.

3. Methodology

3.1. Layout of boreholes drilled in underground coal mine

In total 8 boreholes at 4 different locations have been drilled from the floor of the mining gallery to obtain samples from and to perform geostress and permeability measurements of the No. 2 coal seam within the MFQ fault zone (Fig. 3a). At each site 2 boreholes with different drilling angle have been drilled at 10, 20, 30, and 50 m (are named B1, B2, B3, B5, respectively) distance from the MFQ fault footwall slip surface (Fig. 3b). These boreholes are drilled from the floor of the mining gallery to penetrate the upper No. 2 coal seam until the whole coal, and the gas flow velocity, gas content are tested in the field (Fig. 3c). Coal samples were characterised in the laboratory conducting proximate analysis, Protodyakonov strength, gas emission index and pore volume tests. Further coal samples were collected from the boreholes and the ribs of the mining gallery at a distance 150 m, 300 m and 500 m from the MFQ fault (F15-1, F15-2, F30 and F50, Fig. 3b).

3.2. In situ permeability of the coal seam

Permeability has been determined from the boreholes intersecting the coal seam. In a first step, the formation gas pressure was determined after sealing the borehole. Then, coalbed gas fluxes were measured at different time steps after releasing the original gas pressure to ambient pressure. Finally, coalbed permeability was obtained using methodology described in Li et al. (2013).

3.3. Mercury porosimetry analysis

Mercury porosimetry analysis was performed following the Chinese Oil and Gas Industry Standard SY/T 5346-1994, using a Micrometrics AutoPore IV 9500 porosimeter, which automatically registers pressure, pore diameter, intrusion volume, and surface area. Before conducting the porosimetry analysis, all samples were dried at 105 °C for 12 h. The

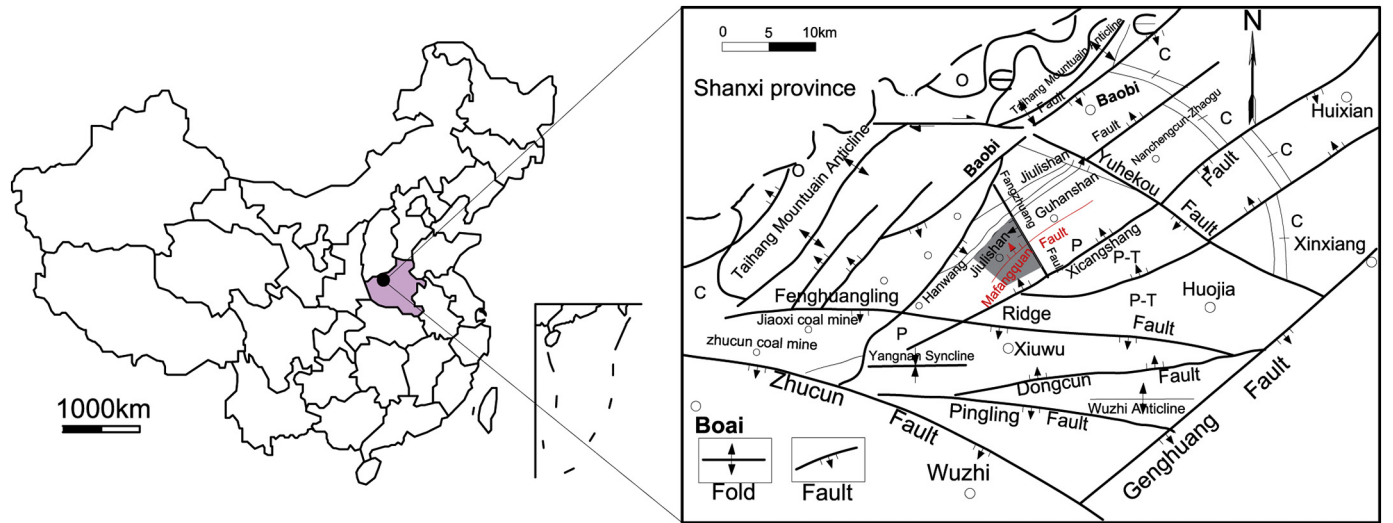


Fig. 1. Structural setting of the Jiaozuo coalfield. The Jiulishan coal mine is located in the centre of this coal field (shaded area), and the normal Mafangquan (MFQ) fault is indicated by the red line, transecting the coal mine in a NE-SW direction and dipping to the NW.

method determines pore diameters of ~10 nm to ~11,000 nm over a pressure range from 0.13 to 140 MPa.

3.4. Protodyakonov strength

Outburst-prone coals have lower strength values than microstructurally unaltered coals (Beamish and Crosdale, 1998; Cao et al., 2001). One of the strength values used in prediction of coal and gas outbursts is the Protodyakonov strength parameter (Lama and Bodziony, 1996; Protodyakonov, 1962). This is a simple test meant to determine the degree of pulverization of coal. This test is performed by dropping a steel plunger (2.4 kg weight) from a height of 6 cm into a cylinder of 76 mm internal diameter that contains ~50 g of coal. This is done 15 times in the case of coal and the crushed sample is sieved through a 0.5 mm mesh. The < 0.5 mm sample is collected and filled in a volumometer whereby the height in the volumometer is measured. Protodyakonov impact strength index I_f is determined by

$$I_f = \frac{20n}{h}$$

where n is the number of impacts and h the height of the fines column in the volumometer (Ghose and Chakraborti, 1986).

3.5. Gas emission index

The gas emission index (ΔP) indicates outburst tendency, following the Chinese Standard of Gas Emission Index (AQ1080-2009). In the procedure used for the present study, 3.5 g coal with a particle size of 0.25–0.5 mm is vacuum-dried at 105 °C and then charged with 1 bar of CH₄ for 1.5 h in a closed system. Excess methane is then evacuated from the system, triggering the gas to desorb, leading to a pressure build-up. Subsequently, the increasing pressure in the system is measured at time intervals of 10 and 60 s. The gas emission index ΔP typically varies between 10 and 60 mmHg (0.013 to 0.08 bar), and is calculated by the pressure difference between the measurement after 60 s and after 10 s respectively.

3.6. In-situ gas content

Coalbed gas content was determined from desorption tests during the geological exploration in accordance with the China Safety Industry Standards (AQ1066-2008; MT/T77-1994):

$$X_0 = \frac{V_1 + V_2 + V_3 + V_4}{Q}$$

where X_0 is the total gas contents [ml.g⁻¹], V_1 is the desorption gas content in the mine [ml], V_2 is the lost gas content [ml], V_3 is the gas content following desorption in a closed vessel [ml], V_4 is the gas content obtained following sample grinding [ml], and Q is the coal sample mass (g). V_2 was obtained from an empirical formula, while V_3 and V_4 were determined in the laboratory. Gas volume was converted to standard conditions (0 °C and 101.3 kPa).

3.7. Stress-relief method for in-situ stress test

A common method to determine in-situ stress state in subsurface mines is to perform stress relief tests by overcoring (Ljunggren et al., 2003). Borehole strains induced by overcoring were determined using hollow inclusion cells. For this, dedicated boreholes were drilled horizontally into the host rock with a length of about 8–12 m, i.e. 3–4 times the adjacent opening width to ensure that the stress state in the measuring position was not locally disturbed by mining activities. During overcoring, the strain changes sensed by every gauge in the hollow inclusion were transmitted to the Wheatstone bridge unit and the output voltage values from the unit, i.e. from all the bridges, were automatically recorded by a programmed data logger. Targeted parameters of the indirect methods can be calculated according to Ljunggren et al. (2003).

4. Results

4.1. Coal properties in fault zone

The coal samples at 11 locations (from mining face and boreholes) away from the MFQ fault were collected using drill cores. Coal samples were sealed to prevent moisture loss and analysed within weeks after sampling. It was found that ash and moisture contents of the coal samples show a similar trend of decreasing values away from the fault damage zone into the coal formation (Fig. 4). Here, ash contents decrease from values as high as 28% near the fault zone (interval of ~20 m) down to about 8% up to 500 m away from the fault. Over the same distance, moisture content decreases from 1.5% to 4.8%. Compared to the undisturbed coal at > 200 m away from the damage zone, the ash content of close to the fault is increased, likely being affected by the fault damage zone.

Gas content, Protodyakonov strength, and gas emission index of

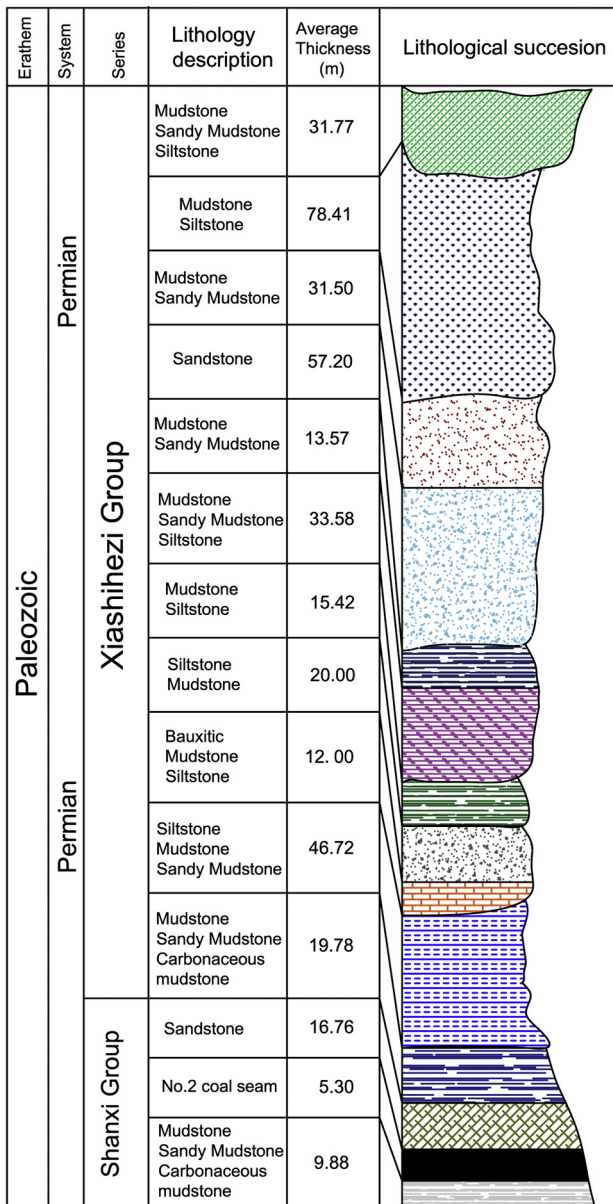


Fig. 2. Stratigraphic column of the Permian coal-bearing strata in the Jiulishan coal mine.

coal samples are equally tested with distance from MFQ fault (Fig. 5). It is obvious that all properties increase with increasing distance from the hanging wall of MFQ fault. Gas content, Protodyakonov strength, and gas emission index close to the fault are $11 \text{ m}^3 \cdot \text{t}^{-1}$, 0.4 and 19 mmHg and increase to $18 \text{ m}^3 \cdot \text{t}^{-1}$, 0.6 and 30 mmHg at a distance of 50 m from the fault, respectively. At a distance of 150 m from the fault, gas content Protodyakonov strength, and gas emission index approach approximately $22 \text{ m}^3 \cdot \text{t}^{-1}$, 0.65 and 31 mmHg. All values increase values that are representative of undamaged coal further away from the fault.

Fig. 5(d) presents the porosity obtained from Hg porosimetry data for the coal samples. Generally, the porosity is around 4% at 10–20 m from the fault, increasing at a distance of 30–50 m from fault to values of 5%–6%. The coal porosity varies from 3.7% to 4.0% over 150 m from the fault, which is similar to the values near the fault.

4.2. Permeability along the fault

In-situ permeability of the MFQ fault zone in Jiulishan coal mine was estimated using methane flow recession curves and pore pressure

observations in boreholes at different distances from the fault. The methane flow rate is high within the first ten minutes; a fast decrease in flow rates is observed for all boreholes (Fig. 6). The borehole at about 10 m from the fault has the highest flow rate, rates further away decrease gradually, and boreholes with a distance of > 30 m from the fault core show constant values, interpreted as the undisturbed permeability of the coal seam. This translates into permeabilities for short distances to the fault of 0.04 to 1.43 mD ($0.04\text{--}1.42\text{E-}15 \text{ m}^2$), and permeabilities for distances of > 30 m of 0.005 to 0.008 mD ($5\text{--}8\text{ E-}18 \text{ m}^2$), about 2.5 orders of magnitude lower than close to the fault. The permeability of the original coal seam, close to the screened depth, ranges from 0.003 to 0.004 mD ($3\text{--}4\text{E-}18 \text{ m}^2$). The permeability observed in this study reflects the complex fault zone permeability structure of the MFQ fault zone.

4.3. Stress test and numerical analysis

4.3.1. In-situ stress test

Using the stress relief test by the overcoring method, in-situ stress measurements were conducted at 5 sites in Jiulishan coal mines, as shown in Fig. 3. The two sites (FGS1 and FGS2) are adjacent to the footwall of the MFQ fault for fault local stress; the three other stress data points show the regional tectonic stress without being impacted by the fault. The depth of these test sites varies from 230 m to 413 m. The formation stress data is shown in Table 1, in which, σ_1 and σ_3 are the maximum and the minimum principal stresses, respectively, and σ_2 is the intermediate stress. The maximum and minimum stress magnitudes range from 12.4 MPa to 18.3 MPa and from 4.9 MPa to 9.2 MPa between 230 and 424 m depth respectively. The maximum and minimum principal stresses are almost horizontal and the intermediate principle stress almost vertical. The three principal stresses are calculated by the overcoring method between horizontal and vertical principal and in-situ stress. The recent in-situ stress field is $\sigma_H > \sigma_V > \sigma_h$ in all 5 test sites, indicating a strike-slip fault regime, while the fault was originally formed as a normal fault. The orientation of σ_H is SW, and concentrated between $S15^\circ\text{W-S}45^\circ\text{W}$, indicating a SSW trending tectonic compressive stress field. In general, both minimum and maximum horizontal stress magnitudes increase linearly with depth, however, the stress in the MFQ fault zone shows some deviation from this linear behaviour (Fig. 7).

The orientations of σ_1 , σ_2 and σ_3 in the five boreholes are also presented in Table 1 and Fig. 7. The primary orientation of σ_1 in the regional (not fault-affected) stress state is NNW. This changes near or at the fault where σ_1 follows a NS direction. Stress rotation near the fault is causing the azimuthal angle to change quite substantially while the dip angle remains largely unaffected. It can be seen that the orientation of σ_1 , σ_2 and σ_3 in FGS1 and FGS2 boreholes is very different to the other orientations, the σ_1 direction away from the fault is approximately $S30^\circ \pm 15^\circ\text{W}$ compared to close to the fault where it rather follows a $S15^\circ \pm 2^\circ\text{E}$ direction and is mostly perpendicular to the fault slip surface. The orientation of σ_2 and σ_3 are rotated by $120^\circ \pm 10^\circ$ rotation compare to GS1, GS2 and GS3, indicated from borehole stresses.

4.3.2. Numerical simulation of stress field

Numerical simulation is a powerful tool to investigate the fault stress and fault zone evolution (Chemenda et al., 2016; Li et al., 2012). Based on the geological conditions of the MFQ fault, FLAC^{3D} was used for mechanical modelling (Itasca, 1997). The software performs mechanical and strain state analysis of geological discontinuous surfaces such as faults, joints and underground mining. We obtained the stress state of the MFQ fault according to the measured stress values by including two damage zones in the hanging and footwall respectively which are 50 m and 100 m in width. The fault zone has a lower mechanical strength compared to the undisturbed zone, hence a mechanical fault zone weakening method was used to build the physical model. The isotropic material around the fault zone, its elastic

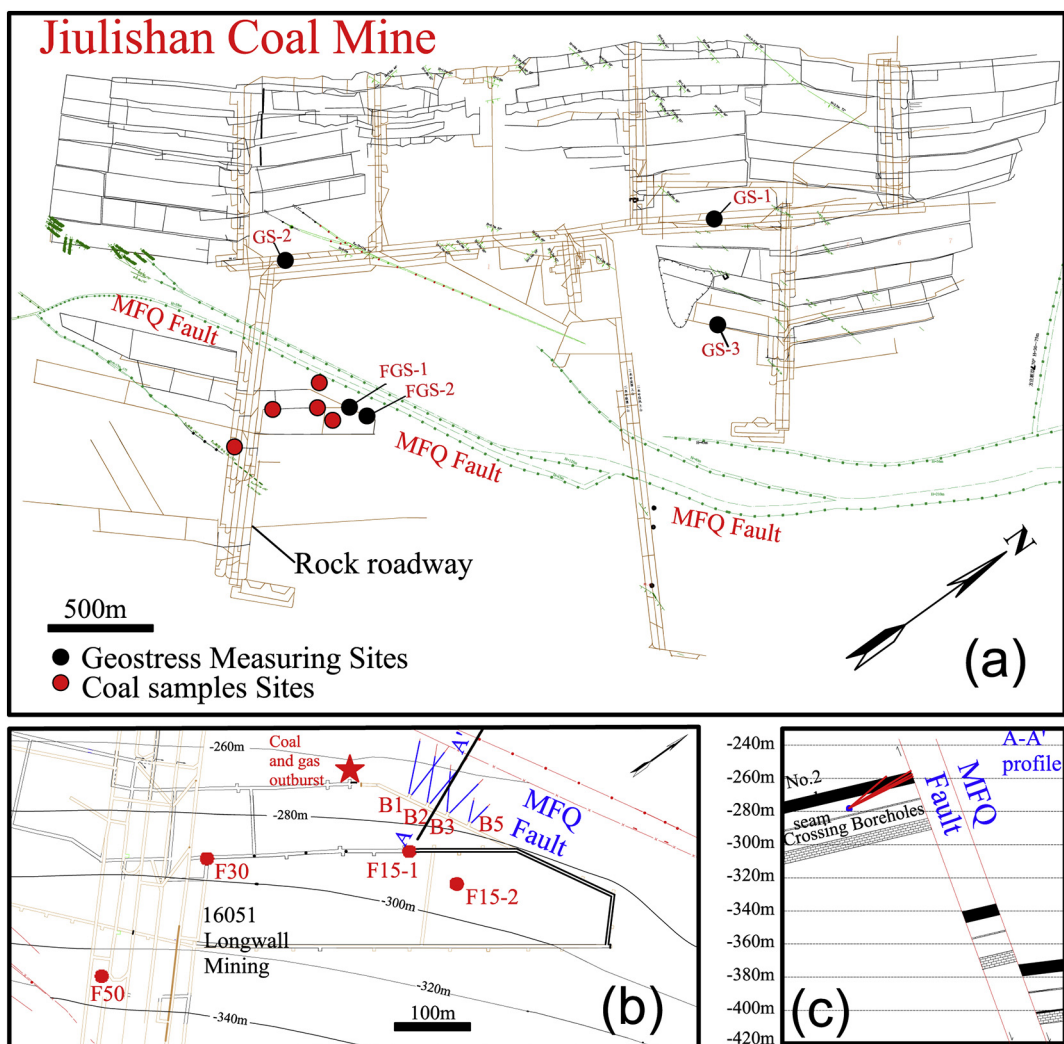


Fig. 3. Locations for coal samples collection, field tests and in-situ stress measurements. (a) Red dots represent sampling locations, black dots show the in-situ stress points. FGS-1 and FGS-2 are within the damage zone of the MFQ fault, GS-1, GS-2 and GS-3 are located far from the MFQ fault to collect regional stress states. (b) detailed location of coal sample, B1, B2, B3 and B5 collected from boreholes at a 10, 20, 30 and 50 m from the MFQ fault footwall slip surface, respectively. Samples F15-1, F15-2, F30 and F50 are collected from boreholes and the coal tunnelling face at 150 m, 300 m and 500 m from the MFQ fault, respectively. A major coal and gas outburst incident in 2011 is shown by the star. (c) A-A' profile from (b) providing an illustration of fault throw and different angles of well drilling from same location. (For interpretation of the references to colour in this figure legend, the reader is referred to the web version of this article.)

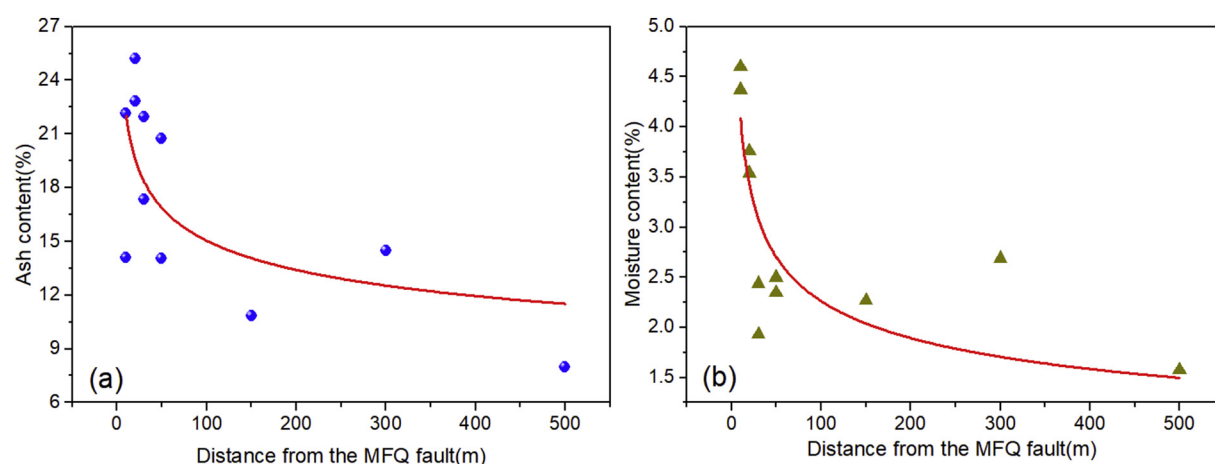


Fig. 4. Ash content (a) and moisture content (b) of coal samples in relation to distance from MFQ fault.

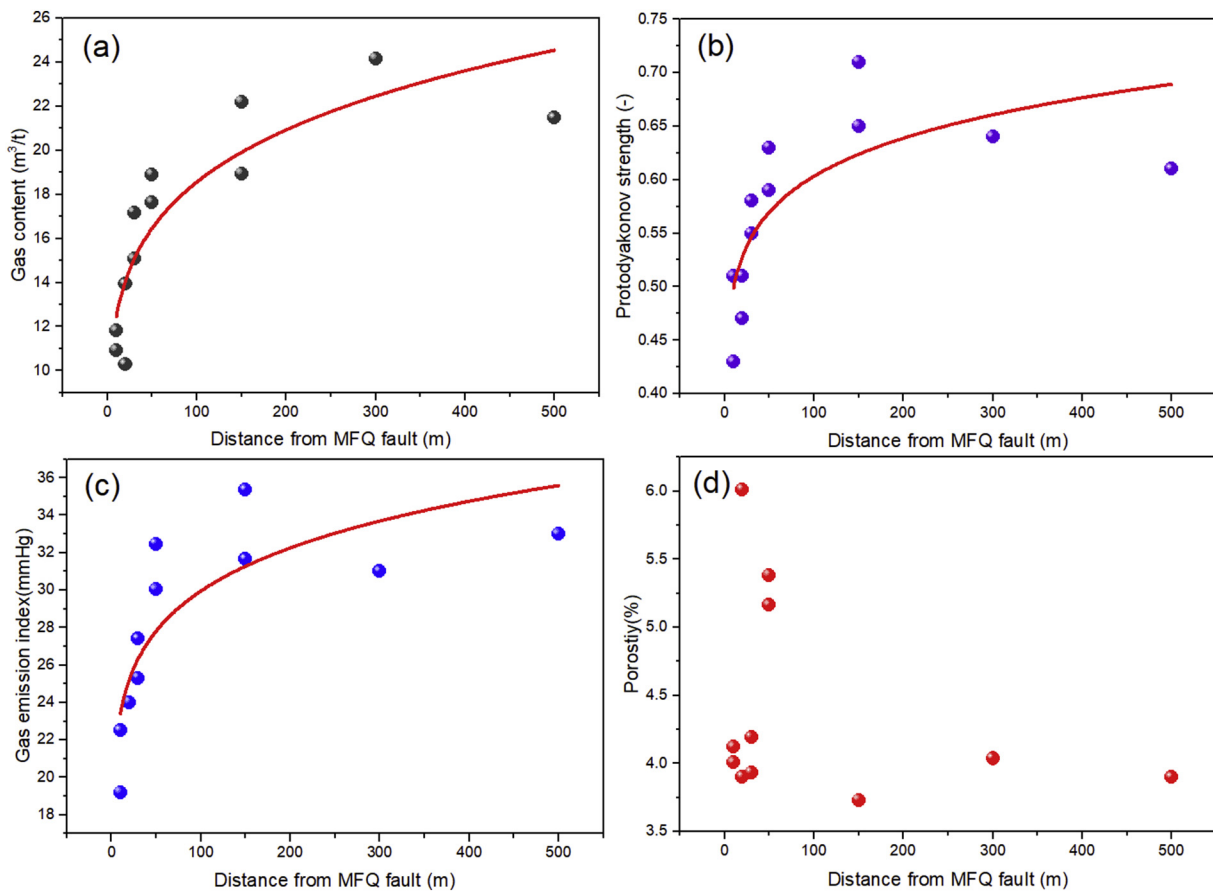


Fig. 5. (a) Gas content, (b) Protodyakonov strength, (c) gas emission index, and (d) porosity with distance from MFQ fault.

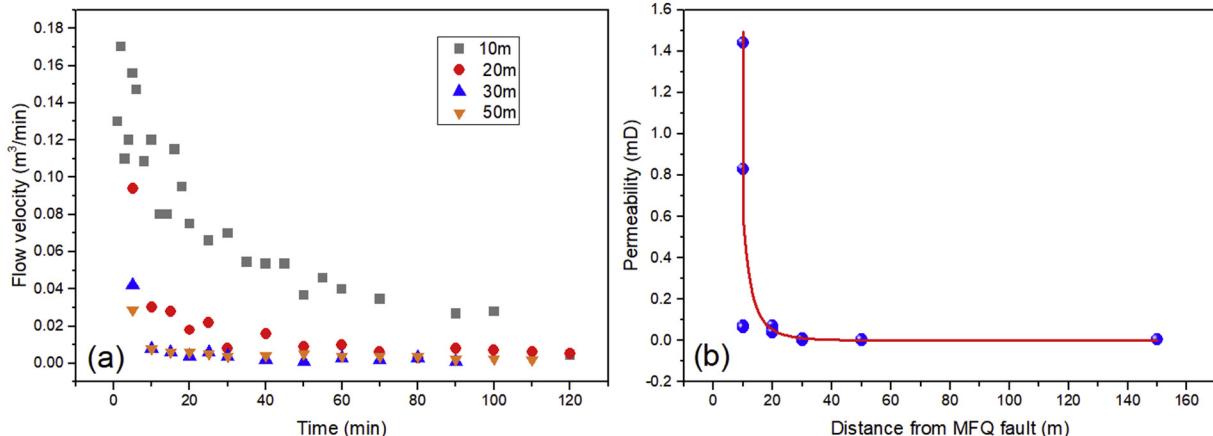


Fig. 6. (a) Methane flow rates determined in the boreholes, and (b) in-situ permeability of boreholes with different distances to the fault.

properties and the regional stress state are implemented in the model using values discussed above. This divides the modelled section into seven layers following the general stratigraphy and fault zone testing through boreholes, the mechanical parameters of rock and fault zone derived from the geological report and experiment results as shown in Table 2.

The maximum principal ($N42^\circ E$) and minimum principal stress direction ($N48^\circ W$) are x and y -axis respectively, and the modelled area is $6000 \times 3000 \times 400$ m in x , y and z direction respectively, corresponding to 100–500 m depth. The dip angle of the coal seam and interbedded layers is 12° . The boundary conditions of the model is applying vertical displacement constraints in z direction, with imposed

stresses along x and y directions. Initially, the fault zone has the same mechanical properties as surrounding lithologies. After the original stress field is produced, new mechanical properties with lower mechanical strength are imposed on the two fault zone demonstrating the influence on the stress field. Furthermore, the boundary stress loading conditions have been fixed after the simulated result in accordance with the five geostress points. The infiel test stress of 15.2 MPa and 6.1 MPa are applied in the xx and yy direction on the model boundary, respectively. The Mohr-Coulomb failure criterion is used to evaluate the failure of the coal and rocks caused by the MFQ fault.

Compared to the in-situ stress test points, the numerical results of stress magnitudes show slight deviations (Fig. 8), indicating that the

Table 1
In-situ stress from the field test in the Jiulishan coal mine.

Sites no.	Depth (m)	Principal stress	Value (MPa)	Dip angle (°)	Azimuthal angle (°)
FGS1	412	σ_1	15.68	-5.28	155.78
		σ_2	8.05	70.59	80.98
		σ_3	6.31	18.62	243.99
FGS2	413	σ_1	14.88	-1.17	157.63
		σ_2	10.92	75.06	72.04
		σ_3	7.1	14.89	247.32
GS1	230	σ_1	12.4	-6.6	226.3
		σ_2	6.1	-62.3	-40.9
		σ_3	4.9	-26.6	120.7
GS2	326	σ_1	14.1	5.8	207.8
		σ_2	6.4	67.8	-55.7
		σ_3	5.1	21.6	112.6
GS3	424	σ_1	18.3	2.7	195.4
		σ_2	9.9	73.2	-47.9
		σ_3	9.2	18.9	117.1

numerical simulation method could reflect a more realistic MFQ fault zone stress state. The maximum principal stress magnitudes for Jiulishan coal mine range between 9.4 and 29.50 MPa, while the minimum principal stress is 2.1 to 10.4 MPa, as shown in the Figs. 9 and 10. The horizontal stress plays an important role in the in-situ stress fields. Stress concentrations at end points or inflection points of the faults are observed with a maximum principal stress of 28.75 MPa, which is 1.7–1.9 times higher than stresses in the intermediate zone. The lower stress area is shown in the fault zone and No.2 coal seam with the maximum principal stress of 9 MPa, which is less than half of the normal stress. In the fault zone, there is a gradient stress increase from fault core to fault damage zone at a distance of 50–150 m from the fault core before stress recovery to the normal regional stress is obtained, which have a relationship with the width of fault damage mechanical properties. This stress magnitude in the fault zone is not only related to the mechanical properties of rock but also to the tectonic stress field.

[Fig. 11 PLACEHOLDER].

[Fig. 11 PLACEHOLDER]

Fig. 11 shows the simulated maximum and minimum principal stress distribution across the MFQ fault, this section location as shown in the Fig. 3b of A-A'. The maximum principal stress increases from values around 10 MPa in the fault core to about 15 MPa in the undamaged host rock. Similarly, the minimum principal stress increases from about 2.3 MPa to 6.1 MPa. The shear stress distribution, as shown in Fig. 12, decreases initially and then increases with an increase in the distance from the fault core. The shear stress is around 4 MPa in the fault

damage zone I (< 50 m), decreases to 2.3–2.7 MPa in the fault damage zone II, and increases again to 4 MPa in the undamaged host rock. The shear stress has a profound impact on the fault stability, slip is likely to occur on a surface if resolved shear stress equals or exceeds the frictional sliding resistance (Moeck et al., 2009; Yamashita et al., 2015). The stress rotation can be found from the stress vectors in Fig. 13. The FGS1 and FGS2 direction angles of maximum principal stress are 140° and 138°, respectively, which are only about 10% lower than the field test values of 155.78° and 157.63°. There is a stress angle rotation when the principle stress approaches the stress in the fault zone, which is typically perpendicular to the fault zone. The closer to the fault zone, the more distinct this trend will be.

5. Discussion

5.1. MFQ fault zone architecture

Fault slip induced deformation and failure to the adjacent coal seam, in combination with mylonitised, granulated and cataclastic coal is found in the fault and related shear zone (Cao et al., 2003; Ju et al., 2005; Li, 2001). This caused a change in the intensity of deformation with distance from the fault slip surface. Following borehole sampling and testing, data was used to define the MFQ fault zone architecture. Consequently, the MFQ Fault Zone in No.2 coal seam is subdivided into three architectural elements (Fig. 14): 1) the fault core, 2) the mylonitized coal zone (Fault damage zone I), which is reconsolidated after fault slip formed powdered coal with a diameter < 1 mm, and 3) the granulated and cataclastic coal zone (Fault damage zone II) at a distance of 50 to 150 m from the fault core. Here, reservoir stress resulted in compaction of this unconsolidated granulated coal.

In general, fault cores are characterised by non-cohesive fault rocks with random fabric, characterised by tectonic stress reduction in grain size and possibly cementation due to mineral precipitation induced by fluid circulation during faulting (Brogi, 2008). Brecciated and mylonitised rocks are observed at depths of 400 m by exploration drillings in the MFQ fault zone, and moisture content increases away from the fault core. The lower water bearing carbonate group is displaced by the MFQ fault. This has an impact on the coal moisture content through the connected fault core, shown in Fig. 3. The composition and rock type of the fault core is contributed to a localized conduit or combined conduit-barrier according to Caine et al. (1996).

In the damage zone, the variation of gas content, gas emission index, as well as moisture and ash contents of coal samples implies that the coal formation differs in properties around the fault core which is

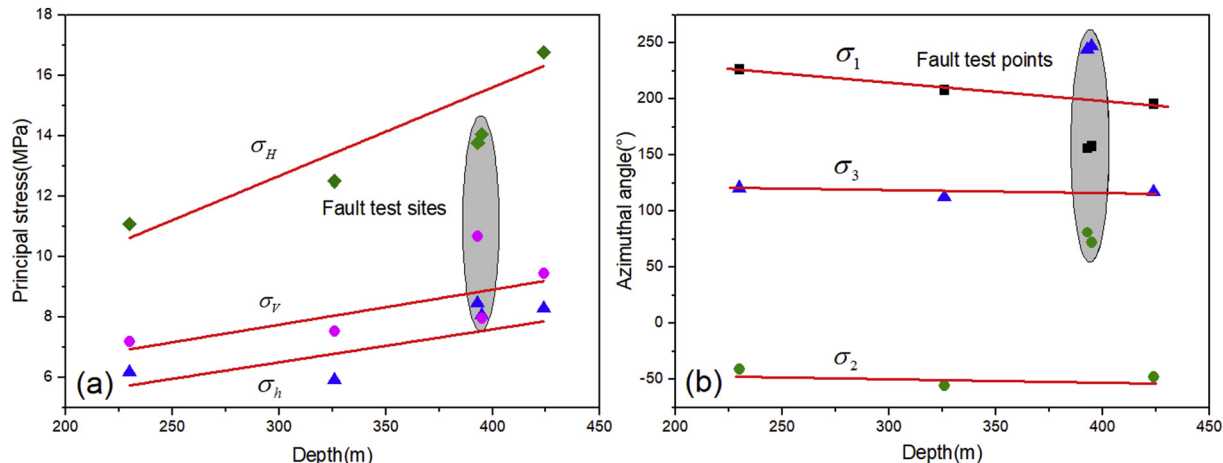
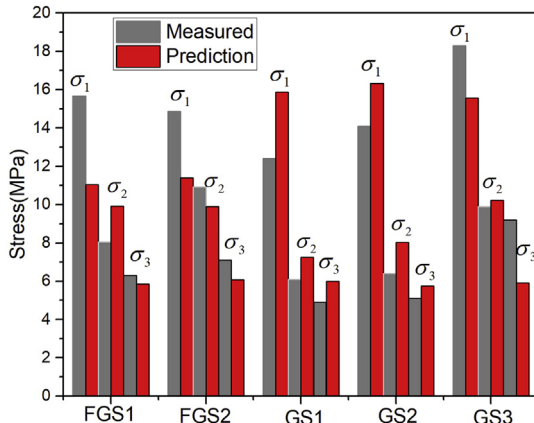


Fig. 7. Measured in-situ stress distribution and comparison between local MFQ fault zone stress magnitudes and regional stresses. (a) stress magnitude, (b) stress azimuthal angle.

Table 2

Thickness and mechanics parameters of the strata.

Lithology	Density [kg.m ⁻³]	Bulk modulus [GPa]	Shear modulus [GPa]	Cohesion (MPa)	Friction angle [°]	Tensile strength [MPa]
Gravel	1940	2.80	1.22	0.60	21.00	0.20
Gritstone	2700	12.88	6.64	17.20	32.80	3.40
Sandstone	2440	12.78	6.24	8.00	24.00	3.20
No.2 coal	1400	2.19	0.95	2.90	20.00	1.30
Sandstone	2440	12.78	6.24	8.00	24.00	3.20
Limestone	2480	14.00	8.40	16.70	28.00	3.90
Fault zone I	1200	0.33	0.36	0.63	37.00	0.80
Fault zone II	1300	7.62	4.40	4.90	34.00	1.20

**Fig. 8.** Comparison between the field test stress and the numerical simulation results.

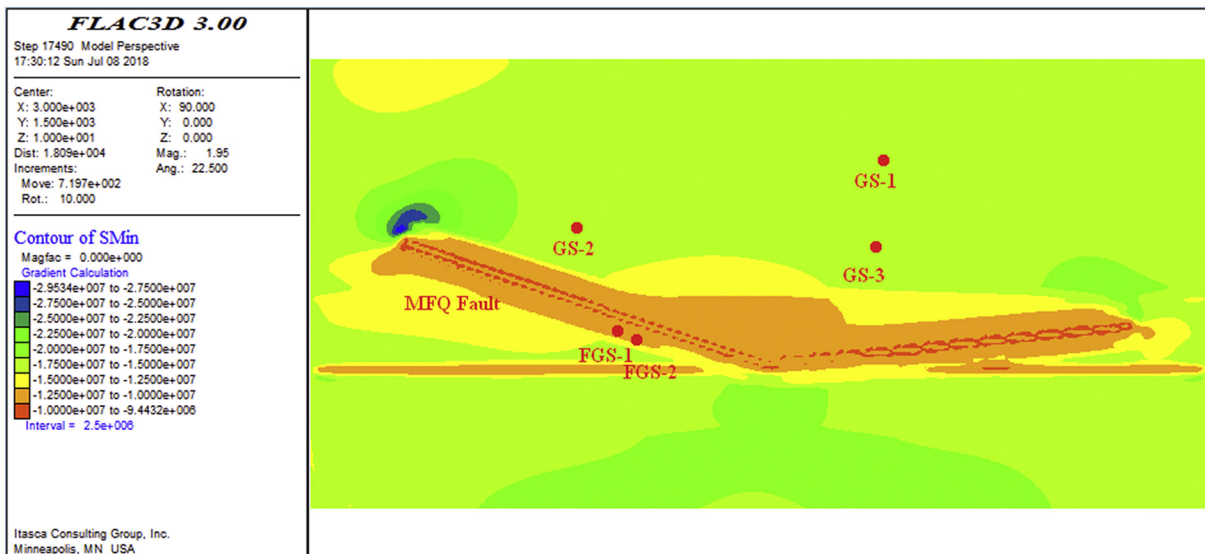
affected by the faulting process. The in-situ gas content and gas emission index show lower values close to the fault compared to 50 m or more from the fault, which is confirmed by the higher moisture and ash content of coal samples adjacent to fault. We interpret the higher ash contents due to fluid circulation and mineral (e.g. carbonate) precipitation in the immediate vicinity of the fault core. Mylonitisation may have increased (micro)fracture porosity in and near the fault core, leading to slightly higher moisture contents. Similar observations have been reported earlier for siliciclastic or carbonaceous fault core material compared to the undeformed protolith (Caine et al., 1996; Zhao et al., 2007).

In the mylonitized coal zone, coal acts as a soft rock compared to the over or underburden, which is dominated by silicate and carbonate minerals. Hence coal porosity increase might be attributed to the formation of microfractures near the fault core. An additional decrease in coal strength due to plastic deformation results in disappearance of the original coal structure (Ju et al., 2005), and the mylonitised coal structure can even be observed in hand specimen.

Most of the fault zone research provides a multiscale qualitative description of fracture density, fracture orientation, fracture length and aperture surrounding a fault core from outcrop studies (Johansen et al., 2005; McGrath and Davison, 1995; Reyer et al., 2012). However, the MFQ fault outcrop studied is studied at a depth of nearly 200 m, so the coal sampling and well testing are carried out without field scale analysis. As a consequence, the fault zone in the coal seam may have a more complicated structure following multiphase tectonic movements, which may have an effect on coal seam deformation (Bo and Yiwen, 2004; Frodsham and Gayer, 1999). This research provides a simple fault architecture to reflect the coal deformation and microscopic features. Further studies are required to better characterise and understand fault zones in coal seams.

5.2. Fault zone stress rotation and permeability structure

The numerical modelling of the stress magnitudes in and surrounding the MFQ fault zone is based on the measured in-situ stress at five different locations within the mine. Generally, at the tip area of the fault, the stress increases significantly, and at either side of the fault, the stress decreases according to the maximum and minimum principal stress state, which have a distance of 50–150 m from the fault core before the stress approaches the normal regional stress (Figs. 9 and 10).

**Fig. 9.** Maximum principal stress of MFQ fault zone.

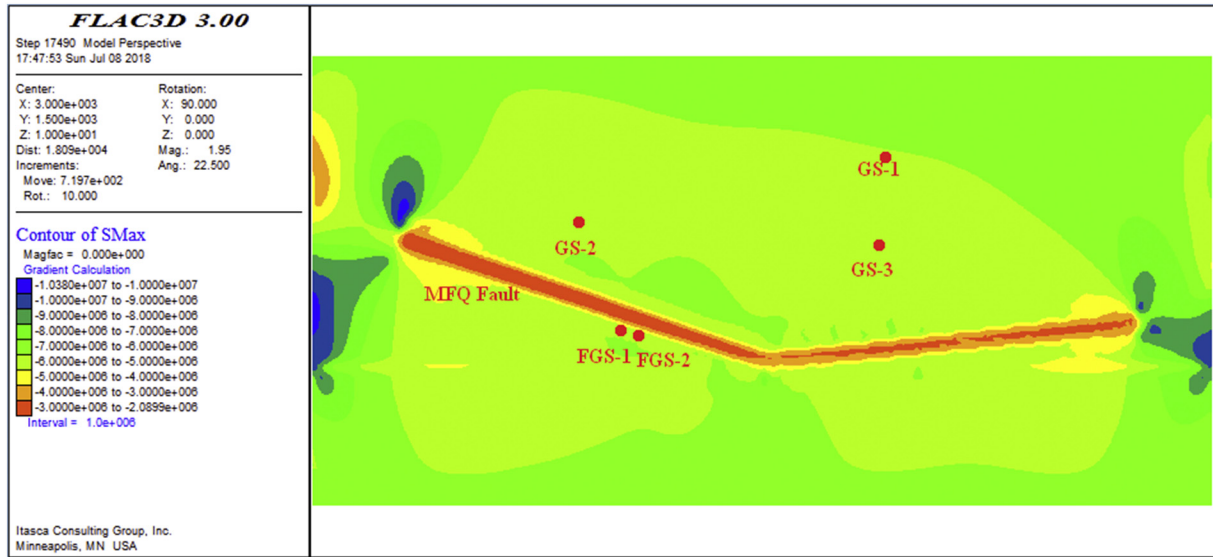


Fig. 10. Minimum principal stress for MFQ fault zone.

A rotation of the maximum principal stress was found in the vicinity of MFQ fault footwall, and stress rotations around faults have been inferred from other seismological studies (Hardebeck and Hauksson, 1999; Rajabi et al., 2017). The borehole outbreak rotation might occur on planes of weakness, such as fractures, faults and bedding planes, at or near the borehole (Martin and Chandler, 1993). The damage zone has a different static elastic modulus and Poisson's ratio with respect to increasing crack damage from the mylonitized to the cataclastic coal zone (Wang et al., 2015; Yin et al., 2015a), and the same coal mechanical property change from low to high pore pressures (Yin et al., 2015b). Modelled stress rotations are substantial and can have important implications for fault zones mechanics (Faulkner et al., 2006), stress rotations are calculated according to a remote stress applied at an angle $\theta = 80^\circ, 60^\circ, 45^\circ$ and the elastic stresses and strains calculated in the remaining layers of fault zone (Fig. 15) (Jaeger et al., 2009).

The influence of Young's modulus E and Poisson's ratio ν on θ is shown by decreasing Young's modulus and increasing Poisson's ratio close to the fault core. These curves were calculated using an applied

remote stress of $\sigma_1 = 15$ MPa (applied at $80^\circ, 60^\circ, 45^\circ$ to the fault zone) and $\sigma_3 = 6$ MPa. In Fig. 12, the effect of Poisson's ratio and Young's modulus in the isotropic model are significant for the case of highly non-oriented faults ($\theta = 60^\circ$ outside the fault). For $E < 3.7$ GPa or $\nu > 0.33$, the rapid increase in the component results in a decrease of θ to values $< 40^\circ$. At the isotropic limit of $\nu = 0.37$, θ can be as low as 20° . Note also that decreasing values of ν result in increasing values of θ , i.e., σ_1 can rotate away from the fault. The stress magnitude and rotation angle are changed when the stress approaches stress values of the fault zone with the original stress not perpendicular to the fault strike. Similar behaviour is observed in other case studies (Hardebeck and Hauksson, 1999; Huang et al., 2014). The stress rotation of the maximum principal (horizontal) stress is small near the fault and the normal stress decreases while the shear stress increases near the fault zone. Furthermore, the shear stress is closely related to the mechanical properties of the fault damage zone as show in Section 4.3.2, potentially increasing the risk of fault slip.

Generally, the permeability architecture of a mature fault zone

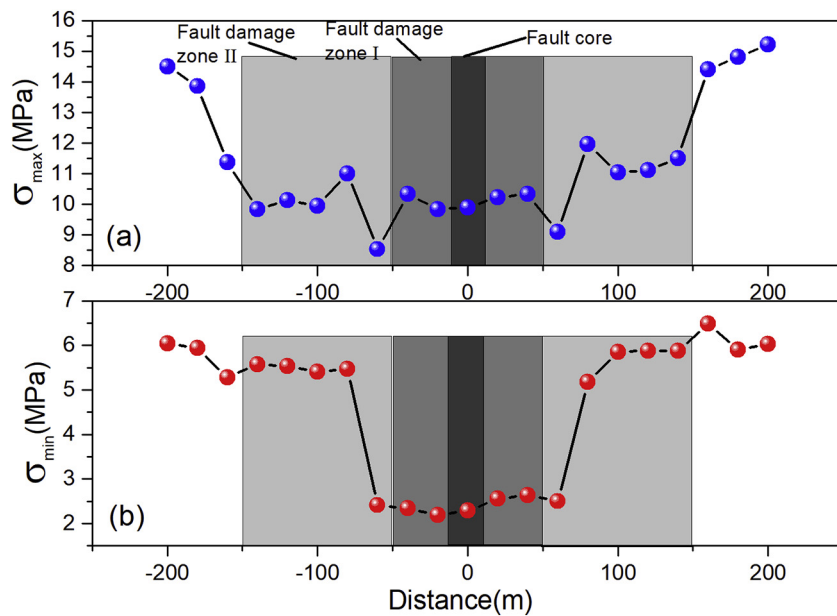


Fig. 11. Simulation results of maximum (σ_1) and minimum (σ_3) principal stress distribution across MFQ fault.

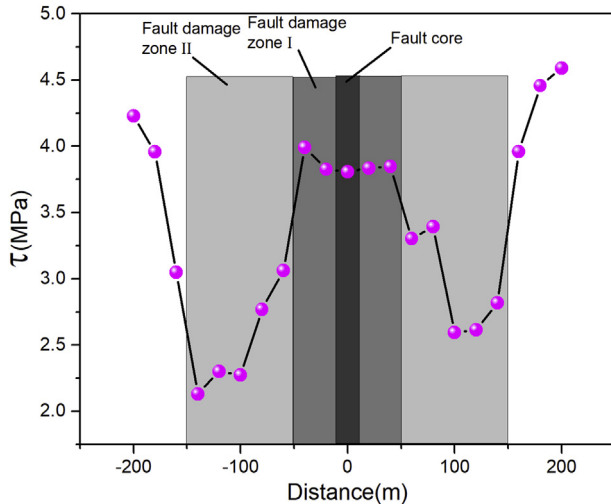


Fig. 12. Shear stress distribution in the fault section, the shear stress is calculated according to $\tau = (\sigma_1 - \sigma_3)/2$, and σ_1 , σ_3 are obtained from numerical calculation.

consists of two main components: the damage zone, which has the highest permeability, and the fault core, which constitutes a low-permeability sector. However, the permeability of the fault zone is changing temporally and spatially. The relationship between permeability and fracture porosity can be described by a cubic law relationship (Peters, 2007):

$$\frac{k}{k_0} = \left(\frac{\phi}{\phi_0} \right)^3$$

where k is the coal permeability, k_0 is the initial permeability, ϕ is the current porosity, ϕ_0 is the initial porosity of coal.

Changes in porosity due to deformation are controlled by alterations in coal grain size and grain size distributions and by the production of microstructures which can modify pore connectivity. Increases in porosity can occur through formation of (micro)fractures and dilatancy associated with coal cataclasis and distress (Chen et al., 2014; Konecny and Kozusnikova, 2011). Coal is a soft material compared to

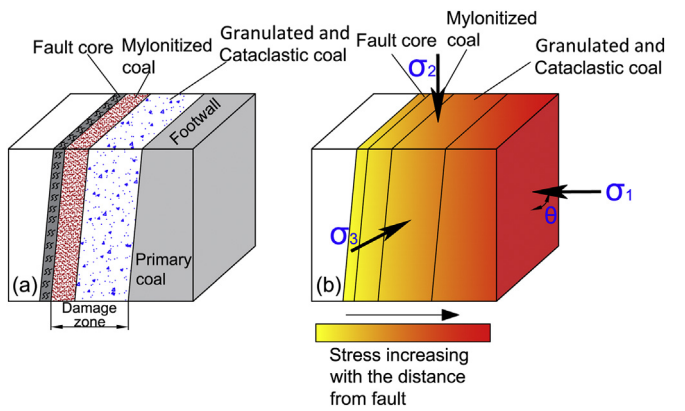


Fig. 14. (a) Architecture of MFQ fault zone in the foot wall. (b) stress regimes in the MFQ fault zone, whereby stress magnitude is decreasing closer to the fault core.

surrounding silicate and carbonate rich layers; the coal powder is found in the fault zone, with an isotropic permeability dominated by millimeter-sized particles under in-situ stress, and the permeability of coal seam under effective stress could be expressed with the in-situ stress and pore pressure (Cui and Bustin, 2005):

$$\frac{k}{k_0} = \exp\{-3C_f[(\bar{\sigma} - \bar{\sigma}_0) - (p - p_0)]\}$$

where k is permeability; C_f is fracture compressibility constant. $\bar{\sigma}$ is the average confining pressure; p is the gas pressure; subscript '0' represents the initial value.

The coal seam damage zone of the MFQ fault has the highest permeability in the mylonitic zone, corresponding to higher porosity and lower in-situ stress. Porosity values determined in the laboratory may have lower values than in-situ values, since small samples do not represent fractures and potential mineralisation in the pore space by increased circulation of fluids in the fault zone (Zhang et al., 2007). Within the cataclastic coal zone, juxtaposed on the mylonitic coal zone, permeability decreases rapidly with distance from the fault, and its primary texture has been damaged. This results in slip surfaces and striations, which could be easily broken into granular solid fines with

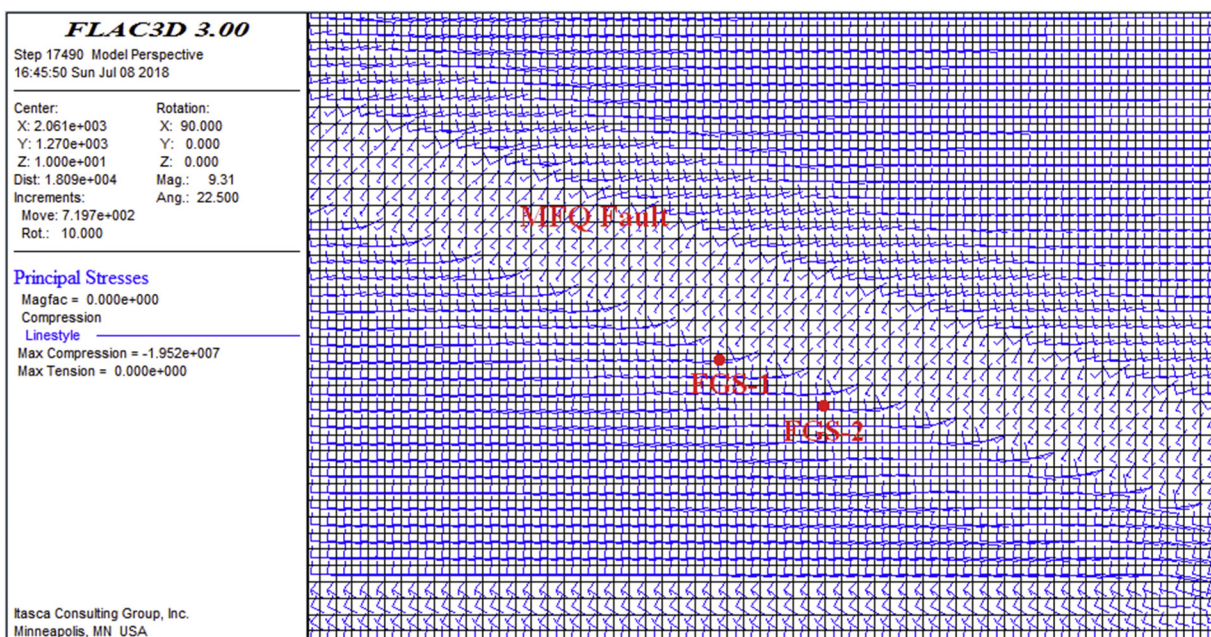


Fig. 13. The trajectory of maximum principal stress when approaching the fault zone.

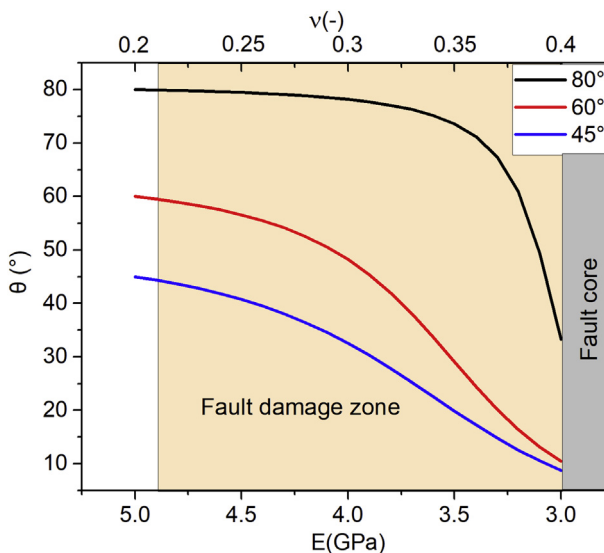


Fig. 15. Graph showing the dependence of σ_1 and θ on Poisson's ratio and Young's modulus for the isotropic multilayer model.

unconsolidated coal. The stress sensitivity and adsorption-swelling effect are attributes to permeability decrease for granulated coal in the MFQ fault zone (Pan and Connell, 2011), the permeability of the fault core may be dominated by the grain-scale permeability of the fault rocks at a constant stress regime, the smaller coal powder have a lower permeability in the mylonitic zone (Taheri et al., 2017). However, fault zone permeability is highly heterogeneous both spatially and temporally under stress change or fault slip.

5.3. Implication for coal and gas outburst

Coal and gas outbursts are dynamic failures resulting in the sudden ejection of thousands of tons of coal and rock as well as large amounts of gas into a limited underground working space and in a short period of time. Outburst of coal and gas is a very complex dynamic phenomenon, which is considered to be the result of the interaction of multiple factors like stress regimes, pore pressure and coal strength. In particular, the stress regime, which is a combination of the in-situ stress and mining-induced stress, consisting of the stress magnitude and principle stress angle as mentioned above, and the pore pressure and coal strength, are recognized to promote or prevent coal and gas outbursts. The understanding of coal and gas outburst is still in the stage of qualitative description instead of quantitative analyses (Yuan, 2016; Zhang et al., 2017). The fault as a geological discontinuity is formed during the tectonic movement and the critical stress regimes, which change the original state of stress, coal structure and the permeability of fault cutting coal seam.

It has been shown that the principle and shear stresses change in the vicinity of the fault damage zone and the undisturbed host rock. Accordingly, there is a stress concentration at the tip of the fault, which may act as the release point for coal and gas outburst. Coal strength in the damage zone is lower than in the intact coal, and is therefore prone to failure under mining induced stress changes. Hence, the coal seam fault damage zone should be detected from coal mechanical properties and coal gas dynamic parameters. This might enable the prediction of the stress state and permeability of fault zone to prevent coal and gas outburst. The gas volume liberated during a gas outburst is usually much bigger than the amount of in-situ gas content in the outburst area, which is regarded as a gas enriched area. The fault zone has a similar structure for gas trapping, a combined conduit-barrier fault core, and gas volumes either adsorbed or as free gas in the porosity are constantly fed from lower coal seams via the relatively permeable fault damage

zone. Therefore, the gas loss rate may be high as $0.1\text{--}0.01 \text{ m}^3 \cdot \text{y}^{-1} \cdot \text{m}^{-1}$, considering an average fault zone permeability of 0.003 mD for long periods of time (Evans and Wong, 1992; Faulkner and Rutter, 2001). The stress state is predicated to develop inside a fault zone of weak material, and an increase in stresses parallel to the displacement direction might suppress hydrofracturing in the case of high pore pressure. In addition, rotation of the principal stress axes typically occurs (Hardebeck and Hauksson, 1999), and a high gas pressure gradient is formed near the exposed surface due to the quick migration of coal gas, which may causes a tensile failure of coal during tunnel excavation (Tu et al., 2018). Moreover, the stress state, which controls the coal and gas outburst, is the most important parameter for outburst prediction, which contains the in-situ stress and superimposed stress induced by mining disturbance stresses. This superimposed stress is characterised before coal excavation takes place using field tests and numerical modelling (An et al., 2013; Wang et al., 2013). However, the stress rotation can also significantly contribute to the tunnel excavation under the in-situ stress field (Sengupta et al., 2013). This can create damage oriented at angles other than the final boundary-parallel crack directions, normally associated with brittle coal damage (Diederichs et al., 2004; Eberhardt, 2001). As a consequence, a profound impact on the tunnelling stability under various mining-induced rotational stress changes and high pore pressure can be observed. To date, this phenomenon has been paid insufficient attention. The in-situ stress state measured at the drill site of MFQ fault shows a nearly strike-slip fault regime rather than normal faulting conditions at the time of deformation. Presumably a normal stress regime would exist prior to the current strike-slip fault regime. However without detailed stress information it is not known how the stress state has changed between initial faulting and present day conditions. Alternatively, the measured stress condition can be used to evaluate the reactivation potential on the MFQ fault (Zoback et al., 2003), which might induce coal and gas outbursts (Islam and Shinjo, 2009; Li et al., 2014; Mazaira and Konicek, 2015). In addition, the coal mining activity could potentially perturb the in-situ stress and rebuild the stress state which, in turn, will have an influence on the fault stress regimes for fault slip risk (Zhang et al., 2018). The energy release during fault slip could further induce to coal and gas outburst at a critical conditions and it is therefore important to understand these relationships in detail.

6. Conclusion

Detailed laboratory and field studies of MFQ fault zone crosscutting coal seam in Jilishan coal mine show that previous conceptual fault zone models are not applicable to the observed fault zone in the coal seam. The porosity, stiffness, gas content of coal samples have a relationship with the distance from the fault, consisting of a fault core, a mylonitized coal zone and a granulated and cataclastic coal zone. Stress measurements indicate a strike-slip fault regime and stress magnitudes decreasing away from the fault core. The observed rotation of maximum and minimum principal stress relative to the regional stress field, and the stress rotation angle also further decrease to become parallel to the fault extension direction. Hence, as indicated from model predictions, the mechanical strength of the fault layer zone changes. The permeability of the fault zone indicates that the mylonitized coal zone has a higher permeability compared to the granulated and cataclastic coal zone. This is consistent with a lower stress state and higher porosity in the mylonitized coal zone. The stress state is an important parameter to predict the permeability of soft coal. The low strength coal, high pore pressure and high local stresses in the fault zone contribute to the potential coal and gas outburst risk. Coal mining induces stress rotation in the tunnel, causing coal failure and/or fault slip, ultimately leading to an increase of the risk of coal outburst. A furthering of the understanding of the in-situ stress rotation as well as the mining related stress rotation in the fault zone is required to reduce this risk.

Acknowledgements

This research was financially supported by the Fundamental Research Funds for the National Science Foundation of China (grant no. 51874295), the Central Universities (grant no. 2015QNA01), and a project funded by the priority academic development program of Jiangsu Higher Education Institutions(PAPD). Thanks to the China Scholarship Council for financially support.

References

- An, F., Cheng, Y., 2014. An explanation of large-scale coal and gas outbursts in underground coal mines: the effect of low-permeability zones on abnormally abundant gas. *Nat. Hazards Earth Syst. Sci.* 14, 2125–2132.
- An, F.-h., Cheng, Y.-p., Wang, L., Li, W., 2013. A numerical model for outburst including the effect of adsorbed gas on coal deformation and mechanical properties. *Comput. Geotech.* 54, 222–231.
- Balsamo, F., Storti, F., Salvini, F., Silva, A., Lima, G., 2010. Structural and petrophysical evolution of extensional fault zones in low-porosity, poorly lithified sandstones of the Barreiras Formation, NE Brazil. *J. Struct. Geol.* 32, 1806–1826.
- Beamish, B.B., Crosdale, P.J., 1998. Instantaneous outbursts in underground coal mines: an overview and association with coal type. *Int. J. Coal Geol.* 35, 27–55.
- Bo, J., Yiwen, J., 2004. Tectonic coal structure and its petrophysical features. *Nat. Gas Ind.* 24, 27–29.
- Bolton, A., Maltman, A., Clennell, M., 1998. The importance of overpressure timing and permeability evolution in fine-grained sediments undergoing shear. *J. Struct. Geol.* 20, 1013–1022.
- Brogi, A., 2008. Fault zone architecture and permeability features in siliceous sedimentary rocks: insights from the Rapolano geothermal area (Northern Apennines, Italy). *J. Struct. Geol.* 30, 237–256.
- Caine, J.S., Minor, S.A., 2009. Structural and geochemical characteristics of faulted sediments and inferences on the role of water in deformation, Rio Grande Rift, New Mexico. *Geol. Soc. Am. Bull.* 121, 1325–1340.
- Caine, J.S., Evans, J.P., Forster, C.B., 1996. Fault zone architecture and permeability structure. *Geology* 24, 1025–1028.
- Cao, Y., He, D., Glick, D.C., 2001. Coal and gas outbursts in footwalls of reverse faults. *Int. J. Coal Geol.* 48, 47–63.
- Cao, Y., Davis, A., Liu, R., Liu, X., Zhang, Y., 2003. The influence of tectonic deformation on some geochemical properties of coals—a possible indicator of outburst potential. *Int. J. Coal Geol.* 53, 69–79.
- Chemenda, A.I., Cavalié, O., Vergnolle, M., Bouissou, S., Delouis, B., 2016. Numerical model of formation of a 3-D strike-slip fault system. *Compt. Rendus Geosci.* 348, 61–69.
- Chen, H., Cheng, Y., Ren, T., Zhou, H., Liu, Q., 2014. Permeability distribution characteristics of protected coal seams during unloading of the coal body. *Int. J. Rock Mech. Min. Sci.* 71, 105–116.
- Crawford, B., Faulkner, D., Rutter, E., 2008. Strength, porosity, and permeability development during hydrostatic and shear loading of synthetic quartz-clay fault gouge. *J. Geophys. Res.* 113.
- Cui, X., Bustin, R.M., 2005. Volumetric strain associated with methane desorption and its impact on coalbed gas production from deep coal seams. *AAPG Bull.* 89, 1181–1202.
- Cuisiat, F., Jostad, H., Andresen, L., Skurtveit, E., Skomedal, E., Hettema, M., Lyslo, K., 2010. Geomechanical integrity of sealing faults during depressurisation of the Statfjord Field. *J. Struct. Geol.* 32, 1754–1767.
- Diederichs, M., Kaiser, P., Eberhardt, E., 2004. Damage initiation and propagation in hard rock during tunnelling and the influence of near-face stress rotation. *Int. J. Rock Mech. Min. Sci.* 41, 785–812.
- Eberhardt, E., 2001. Numerical modelling of three-dimension stress rotation ahead of an advancing tunnel face. *Int. J. Rock Mech. Min. Sci.* 38, 499–518.
- Evans, B., Wong, T.-f., 1992. *Fault Mechanics and Transport Properties of Rocks*. Academic Press.
- Evans, J.P., Forster, C.B., Goddard, J.V., 1997. Permeability of fault-related rocks, and implications for hydraulic structure of fault zones. *J. Struct. Geol.* 19, 1393–1404.
- Fairley, J.P., Hinds, J.J., 2004. Field observation of fluid circulation patterns in a normal fault system. *Geophys. Res. Lett.* 31.
- Faulkner, D.R., Rutter, E.H., 2001. Can the maintenance of overpressured fluids in large strike-slip fault zones explain their apparent weakness? *Geology* 29, 503–506.
- Faulkner, D., Mitchell, T., Healy, D., Heap, M., 2006. Slip on/weak/faults by the rotation of regional stress in the fracture damage zone. *Nature* 444, 922.
- Faulkner, D., Jackson, C., Lunn, R., Schlische, R., Shipton, Z., Wibberley, C., Withjack, M., 2010. A review of recent developments concerning the structure, mechanics and fluid flow properties of fault zones. *J. Struct. Geol.* 32, 1557–1575.
- Fisne, A., Esen, O., 2014. Coal and gas outburst hazard in Zonguldak Coal Basin of Turkey, and association with geological parameters. *Nat. Hazards* 74, 1363–1390.
- Fossen, H., Bale, A., 2007. Deformation bands and their influence on fluid flow. *AAPG Bull.* 91, 1685–1700.
- Frodsham, K., Gayer, R., 1999. The impact of tectonic deformation upon coal seams in the South Wales coalfield, UK. *Int. J. Coal Geol.* 38, 297–332.
- Ghose, A.K., Chakraborti, S., 1986. Empirical Strength Indices Of Indian Coals - An Investigation, The 27th U.S. Symposium on Rock Mechanics (USRMS). American Rock Mechanics Association, Tuscaloosa, Alabama.
- Hardebeck, J.L., Hauksson, E., 1999. Role of fluids in faulting inferred from stress field signatures. *Science* 285, 236–239.
- Huang, M.-q., Wu, A.-x., Wang, Y.-m., Bin, H., 2014. Geostress measurements near fault areas using borehole stress-relief method. *Trans. Nonferrous Metals Soc. China* 24, 3660–3665.
- Islam, M.R., Shinjo, R., 2009. Mining-induced fault reactivation associated with the main conveyor belt roadway and safety of the Barapukuria Coal Mine in Bangladesh: constraints from BEM simulations. *Int. J. Coal Geol.* 79, 115–130.
- Itasca, F.D., 1997. *Fast Lagrangian Analysis of Continua in 3-dimensions, Version 3.0*, Manual. Itasca, Minnesota.
- Jaeger, J.C., Cook, N.G., Zimmerman, R., 2009. *Fundamentals of Rock Mechanics*. John Wiley & Sons.
- Ji, Z.-M., Chen, Z.-J., Pan, J.-N., Niu, Q.-H., 2017. A novel method for estimating methane emissions from underground coal mines: the Yanma coal mine, China. *Atmos. Environ.* 170, 96–107.
- Johansen, T.E.S., Fossen, H., Kluge, R., 2005. The impact of syn-faulting porosity reduction on damage zone architecture in porous sandstone: an outcrop example from the Moab Fault, Utah. *J. Struct. Geol.* 27, 1469–1485.
- Ju, Y., Jiang, B., Hou, Q., Wang, G., 2005. Relationship between nanoscale deformation of coal structure and metamorphic-deformed environments. *Chin. Sci. Bull.* 50, 1785–1796.
- Karacan, C.Ö., Ulery, J.P., Goodman, G.V.R., 2008. A numerical evaluation on the effects of impermeable faults on degasification efficiency and methane emissions during underground coal mining. *Int. J. Coal Geol.* 75, 195–203.
- Karacan, C.Ö., Ruiz, F.A., Cotè, M., Phipps, S., 2011. Coal mine methane: a review of capture and utilization practices with benefits to mining safety and to greenhouse gas reduction. *Int. J. Coal Geol.* 86, 121–156.
- Konecny, P., Kozusnikova, A., 2011. Influence of stress on the permeability of coal and sedimentary rocks of the Upper Silesian basin. *Int. J. Rock Mech. Min. Sci.* 48, 347–352.
- Lama, R., Bodziony, J., 1996. *Outbursts of Gas, Coal and Rock in Underground Coal Mines*. (RD Lama).
- Li, H., 2001. Major and minor structural features of a bedding shear zone along a coal seam and related gas outburst, Pingdingshan coalfield, northern China. *Int. J. Coal Geol.* 47, 101–113.
- Li, H., Ogawa, Y., Shimada, S., 2003. Mechanism of methane flow through sheared coals and its role on methane recovery. *Fuel* 82, 1271–1279.
- Li, W., Cheng, Y.-P., Wang, L., 2011. The origin and formation of CO₂ gas pools in the coal seam of the Yaojie coalfield in China. *Int. J. Coal Geol.* 85, 227–236.
- Li, K., Wang, Y.-y., Huang, X.-c., 2012. DDM regression analysis of the in-situ stress field in a non-linear fault zone. *Int. J. Miner. Metall. Mater.* 19, 567–573.
- Li, W., Cheng, Y.-p., Wang, L., Zhou, H.-x., Wang, H.-f., Wang, L.-g., 2013. Evaluating the security of geological coalbed sequestration of supercritical CO₂ reservoirs: the Haishawan coalfield, China as a natural analogue. *Int. J. Greenhouse Gas Control* 13, 102–111.
- Li, Z., Dou, L., Cai, W., Wang, G., He, J., Gong, S., Ding, Y., 2014. Investigation and analysis of the rock burst mechanism induced within fault-pillars. *Int. J. Rock Mech. Min. Sci.* 70, 192–200.
- Ljunggren, C., Chang, Y., Janson, T., Christiansson, R., 2003. An overview of rock stress measurement methods. *Int. J. Rock Mech. Min. Sci.* 40, 975–989.
- Losh, S., Haney, M., 2006. Episodic fluid flow in an aseismic overpressured growth fault, northern Gulf of Mexico. In: *Earthquakes: Radiated Energy and the Physics of Faulting*, pp. 199–205.
- Lunn, R.J., Willson, J.P., Shipton, Z.K., Moir, H., 2008. Simulating brittle fault growth from linkage of preexisting structures. *J. Geophys. Res.* 113.
- Mark, C., 2018. Coal bursts that occur during development: a rock mechanics enigma. *Int. J. Min. Sci. Technol.* 28, 35–42.
- Marone, C., Scholz, C., 1989. Particle-size distribution and microstructures within simulated fault gouge. *J. Struct. Geol.* 11, 799–814.
- Martin, C.D., Chandler, N.A., 1993. Stress heterogeneity and geological structures. In: *International Journal of Rock Mechanics and Mining Sciences & Geomechanics Abstracts*. Elsevier, pp. 993–999.
- Mazaira, A., Konicek, P., 2015. Intense rockburst impacts in deep underground construction and their prevention. *Can. Geotech. J.* 52, 1426–1439.
- McGrath, A.G., Davison, I., 1995. Damage zone geometry around fault tips. *J. Struct. Geol.* 17, 1011–1024.
- Moeck, I., Kwiatek, G., Zimmermann, G., 2009. Slip tendency analysis, fault reactivation potential and induced seismicity in a deep geothermal reservoir. *J. Struct. Geol.* 31, 1174–1182.
- Moustafa, A.R., Dowidar, H., Yousef, M., 2016. Architecture of fault damage zones of normal faults, Gebel Atqa area, Gulf of Suez rift, Egypt. *Mar. Pet. Geol.* 77, 43–53.
- Pan, Z., Connell, L.D., 2011. Modelling of anisotropic coal swelling and its impact on permeability behaviour for primary and enhanced coalbed methane recovery. *Int. J. Coal Geol.* 85, 257–267.
- Peters, E.J., 2007. *Petrophysics*. University of Texas at Austin, Department of Geology and Ecosystems Engineering, pp. 1049.
- Protodyakonov, M., 1962. Mechanical properties and drillability of rocks, Proceedings of the Fifth Symposium on Rock Mechanics. University of Minnesota, Minneapolis, MN, pp. 103–118.
- Rajabi, M., Tingay, M., King, R., Heidbach, O., 2017. Present-day stress orientation in the Clarence-Moreton Basin of New South Wales, Australia: a new high density dataset reveals local stress rotations. *Basin Res.* 29, 622–640.
- Rawling, G.C., Goodwin, L.B., 2006. Structural record of the mechanical evolution of mixed zones in faulted poorly lithified sediments, Rio Grande rift, New Mexico, USA. *J. Struct. Geol.* 28, 1623–1639.
- Reyer, D., Bauer, J.F., Philipp, S.L., 2012. Fracture systems in normal fault zones cross-cutting sedimentary rocks, Northwest German Basin. *J. Struct. Geol.* 45, 38–51.

- Sengupta, S., Subrahmanyam, D.S., Sinha, R.K., Shyam, G., 2013. Estimation of the impact of mining on stresses by actual measurements in pre and post mining stages by hydrofracture method—a case study in a copper mine. In: Effective and Sustainable Hydraulic Fracturing. InTech.
- Shepherd, J., Rixon, L., Griffiths, L., 1981. Outbursts and geological structures in coal mines: a review. *International J. Rock Mech. Min. Sci. Geomech. Abstr.* 267–283.
- Taheri, S., Ghemesi, S., Kantzias, A., 2017. Permeability calculations in unconsolidated homogeneous sands. *Powder Technol.* 321, 380–389.
- Tu, Q., Cheng, Y., Liu, Q., Guo, P., Wang, L., Li, W., Jiang, J., 2018. Investigation of the formation mechanism of coal spallation through the cross-coupling relations of multiple physical processes. *Int. J. Rock Mech. Min. Sci.* 105, 133–144.
- van der Zee, W., Urai, J.L., 2005. Processes of normal fault evolution in a siliciclastic sequence: a case study from Miri, Sarawak, Malaysia. *J. Struct. Geol.* 27, 2281–2300.
- Wang, S., Elsworth, D., Liu, J., 2013. Permeability evolution during progressive deformation of intact coal and implications for instability in underground coal seams. *Int. J. Rock Mech. Min. Sci.* 58, 34–45.
- Wang, L., Cheng, Y.-P., Liu, H.-Y., 2014. An analysis of fatal gas accidents in Chinese coal mines. *Saf. Sci.* 62, 107–113.
- Wang, H., Pan, J., Wang, S., Zhu, H., 2015. Relationship between macro-fracture density, P-wave velocity, and permeability of coal. *J. Appl. Geophys.* 117, 111–117.
- Wibberley, C.A., Yielding, G., Di Toro, G., 2008. Recent advances in the understanding of fault zone internal structure: a review. *Geol. Soc. Lond., Spec. Publ.* 299, 5–33.
- Wiprut, D., Zoback, M.D., 2002. Fault reactivation, leakage potential, and hydrocarbon column heights in the northern North Sea. In: Norwegian Petroleum Society Special Publications. Elsevier, pp. 203–219.
- Wu, Q., Wang, M., Wu, X., 2004. Investigations of groundwater bursting into coal mine seam floors from fault zones. *Int. J. Rock Mech. Min. Sci.* 41, 557–571.
- Yamashita, F., Fukuyama, E., Mizoguchi, K., Takizawa, S., Xu, S., Kawakata, H., 2015. Scale dependence of rock friction at high work rate. *Nature* 528, 254.
- Yin, G., Jiang, C., Wang, J., Xu, J., 2015a. Geomechanical and flow properties of coal from loading axial stress and unloading confining pressure tests. *Int. J. Rock Mech. Min. Sci.* 155–161.
- Yin, G., Li, M., Wang, J., Xu, J., Li, W., 2015b. Mechanical behavior and permeability evolution of gas infiltrated coals during protective layer mining. *Int. J. Rock Mech. Min. Sci.* 80, 292–301.
- Yuan, L., 2016. Control of coal and gas outbursts in Huainan mines in China: A review. *J. Rock Mech. Geotech. Eng.* 8, 559–567.
- Zhai, C., Xiang, X., Xu, J., Wu, S., 2016. The characteristics and main influencing factors affecting coal and gas outbursts in Chinese Pingdingshan mining region. *Nat. Hazards* 82, 507–530.
- Zhang, S., Tullis, T.E., 1998. The effect of fault slip on permeability and permeability anisotropy in quartz gouge. *Tectonophysics* 295, 41–52.
- Zhang, J., Standifird, W., Roegiers, J.-C., Zhang, Y., 2007. Stress-dependent fluid flow and permeability in fractured media: from lab experiments to engineering applications. *Rock Mech. Rock Eng.* 40, 3–21.
- Zhang, X., Liu, Y., Wang, G., Liu, H., 2009. Coalbed methane resources and reservoir characteristics of NO. II1 coal seam in the Jiaozuo coalfield, China. *Energy Explor. Exploit.* 27, 307–332.
- Zhang, C., Canbulat, I., Hebblewhite, B., Ward, C.R., 2017. Assessing coal burst phenomena in mining and insights into directions for future research. *Int. J. Coal Geol.* 179, 28–44.
- Zhang, Y., Underschultz, J., Langhi, L., Mallants, D., Strand, J., 2018. Numerical modelling of coal seam depressurization during coal seam gas production and its effect on the geomechanical stability of faults and coal beds. *Int. J. Coal Geol.* 195, 1–13.
- Zhao, C., Hobbs, B., Ord, A., Hornby, P., Peng, S., Liu, L., 2007. Mineral precipitation associated with vertical fault zones: the interaction of solute advection, diffusion and chemical kinetics. *Geofluids* 7, 3–18.
- Zoback, M., Barton, C., Brady, M., Castillo, D., Finkbeiner, T., Grollimund, B., Moos, D., Peska, P., Ward, C., Wiprut, D., 2003. Determination of stress orientation and magnitude in deep wells. *Int. J. Rock Mech. Min. Sci.* 40, 1049–1076.